

Zippering, Entanglement, and the Elastic Modulus of Aligned Single-Walled Carbon Nanotube Films

Yoonjin Won¹, Yuan Gao¹, Matthew A. Panzer¹, Rong Xiang², Shigeo Maruyama³, Thomas W. Kenny¹, Wei Cai¹, Kenneth E. Goodson^{1*}

Affiliations:

¹Department of Mechanical Engineering, Stanford University, Stanford, California 94305, USA.

²School of Physics and Engineering, Sun Yat-sen University, Guangzhou 510275, China.

³Department of Mechanical Engineering, The University of Tokyo, Tokyo 113-8656, Japan.

*Correspondence to: goodson@stanford.edu

Keywords: carbon nanotubes, modulus, van der Waals, , and thermal interface material.

Abstract:

Reliably routing heat to and from conversion materials is a daunting challenge for a variety of innovative energy technologies – from thermal solar to automotive waste heat recovery systems - whose efficiencies degrade due to massive thermomechanical stresses at interfaces. This problem may soon be addressed by adhesives based on vertically aligned carbon nanotubes, which promise the revolutionary combination of high through-plane thermal conductivity and vanishing in-plane mechanical stiffness. Here we report the first data for the critical in-plane modulus of aligned single-walled carbon nanotube films using a novel microfabricated resonator method. Molecular simulations and electron microscopy identify the nanoscale mechanisms responsible for this property. The zipping and unzipping of adjacent nanotubes and the degree of alignment and entanglement are shown to govern the spatially varying local modulus, thereby providing the route to engineered materials with breakthrough combinations of mechanical and thermal properties.

Introduction

Main Text: Nanostructured materials provide unique combinations of properties that promise performance breakthroughs for applications ranging from energy conversion to data storage and computation (1-4). In many cases it is the very unusual combination of two properties (5), neither of which is an extreme value when considered alone, that leads to adoption and major performance benefits. An example is the search for a mechanically compliant thermal conductor that can, for example, link semiconducting materials with the metals used for heat spreading and exchange. A particularly compelling case is thermoelectric waste heat recovery systems (2), for which the interfaces between the thermoelectric materials, electrodes, insulators, and heat exchangers must accommodate enormous, repetitive thermomechanical stress. However, nature does not provide a material combining the necessary high thermal conductivity with the required low elastic modulus (6, 7).

Vertically aligned carbon nanotube (CNT) films may combine mechanical compliance with high thermal conductivity (8-12), but there have been few reports of the in-plane modulus of these films and little physical explanation for the wide range for the data (4-300 MPa) (13-15). Our previous data for the thickness-dependent in-plane modulus of multi-walled CNT films indicated a strong dependence on the nanotube density and alignment (15), which are linked to the detailed growth details (16, 17). Other approaches, such as mesoscopic simulations or atomistic models, found that CNT networks exhibit unique self-organization, including bending and bundling (18-20). Therefore, relating the nanoscale morphological details to the mechanical properties is critical.

Combined experimental, theoretical, and computational techniques applied to the more complex and fundamentally challenging single-walled CNT system are presented for the first time in this paper, along with the first in-plane data for the modulus for single-walled CNT films. Since single-walled CNT films have higher densities and smaller tube-tube distances, these films exhibit more complex dynamics and tube-tube interactions than multi-walled CNT films. We present coarse-grained molecular simulations, and this approach is consistent with a much simpler cellular model treating the films as foam. The coarse-grained simulations not only predict the modulus, but also describe the manner in which the nanotubes self-organize into bundles and highly entangled regions due to van der Waals forces. The computational results reveal the significance of deformation mechanisms in determining the mechanical response of the single-walled CNT films.

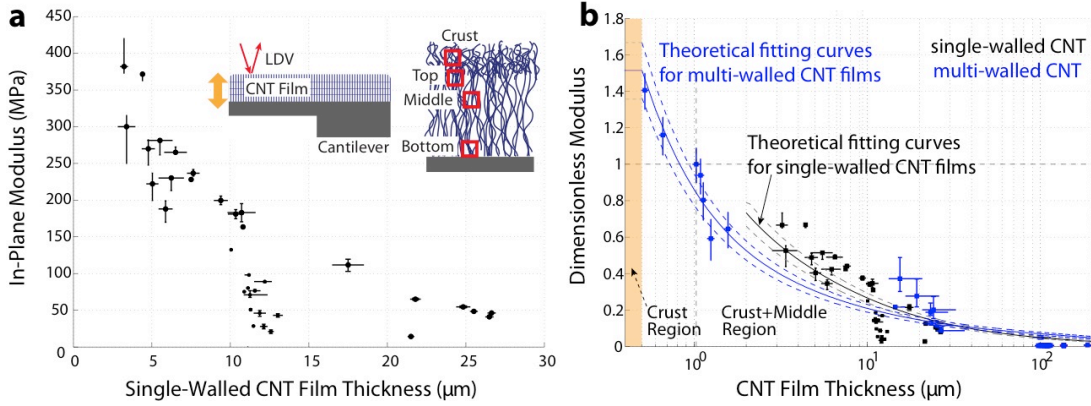


Fig. 1. (a) Effective in-plane modulus ($E_{1,exp}$) of vertically aligned single-walled CNT samples measured using a resonator technique. The thickness variations and the resulting modulus variations due to the nonuniformities in nanotube growth are illustrated by the horizontal and vertical error bars, respectively. (Inset) Schematic of a resonator with a vertically aligned CNT film and a schematic showing the different layers in a film are overlaid on the plot. (b) Dimensionless modulus, $E^* = \frac{E_{CNT}}{E_{ref}} \frac{\rho_{ref}}{\rho_{CNT}}$,

including our past data on multi-walled CNT films (15, 21) and best-fit lines calculated using a three-layer analysis. Dashed lines indicate the effect of varying modulus of the crust (600 MPa) and middle (10 MPa) layers by $\pm 10\%$ on the effective modulus.

The microfabricated resonator depicted in Fig. 1a measures the effective in-plane modulus of single-walled CNT films ($E_{1,exp}$). The measurement method (15) and nanotube growth process (22) are described in the *Supporting Information*. Figure 1a shows that $E_{1,exp}$ decreases with increasing nanotube film thickness, which we attribute to inhomogeneities (with respect to the film-normal coordinate) in the density and alignment. The films have a disordered and dense crust layer on top of an aligned middle region (15, 17, 23), while single-walled CNT films are denser and stiffer. The theoretical curves, shown in Fig. 1b, capture the effect that as the film grows taller, the modulus of the middle layer becomes more dominant, and the overall modulus of the film decreases. The measurements and three-layer model suggest that large differences between the modulus of the crust and middle layer are due to their morphological variations.

To understand the mechanisms governing the mechanical response of the single-walled CNT films, we use two separate simulation methods. The first is a simple model for cellular solids. Since carbon nanotubes are low-density solids, previous studies have shown that the mechanical response and nanostructure of films closely resemble those of a foam or cellular solid (10, 12). Gibson and Ashby introduced a rectangular cellular model that has been widely used to estimate the modulus of foams (24). Since the film structure consists of angled tube segments rather than perfectly horizontal and vertical beams, we present a modified cellular model in which trusses connect the corners and the center of each unit cell, as shown in Fig. 2a (25) (See *Supporting Information*). The aspect ratio (AR) of a unit cell is related to the angle made by the trusses with respect to the horizontal plane, where $AR = H/L = \sqrt{2} \tan \theta$. By considering the bending of the trusses in response to horizontal and vertical forces applied to the film, we can predict the in-plane modulus ($E_{1,cell}$) and out-of-plane modulus ($E_{2,cell}$) of the film as

$$E_{1,cell} = C \sin \theta \cos^4 \theta \cdot (2 - \cos^2 \theta)^{-1} \quad (1)$$

$$E_{2,cell} = C \sin^3 \theta \quad (2)$$

with $C = \alpha E_{truss} I_{truss} f_{truss}^2 A_{truss}^{-2}$, where E_{truss} , I_{truss} , and A_{truss} are the Young's modulus, moment of inertia and cross section area of each truss, and α is a numerical constant. The volume fraction occupied by the nanotubes is $f_{truss} = A_{truss} l / HL^2$ where l is the length of the truss. Since nanotubes tend to bundle together, the trusses in our cellular model do not necessarily represent individual nanotubes. Hence, I_{truss} and A_{truss} in our model are unknown, and constant C in Eq. (2) and (3) is treated as a fitting parameter. Figure 2b plots the predicted dependence of the moduli on the AR at different volume fractions (f) of nanotubes. Our model predicts the f_{truss}^2 dependence of the film moduli as the Gibson and Ashby model, but shows a stronger dependence of the film moduli on the AR. The prediction is largely consistent with our experimental data on the film moduli as well as SEM estimates of the AR and f . The ratio between the predicted $E_{1,cell}$ of the middle and crust layer is consistent with the measurements, which is in the range of 30-60. The cellular model assumes that the elastic deformation of the film is entirely caused by truss bending. In reality, the nanotubes are held together by weak van der Waals forces, and it may be that zipping of nanotube bundles may play a role in the elastic compliance of the film. To remove the empirical fitting parameter C and to gain a deeper understanding on the realistic structure and dynamics of the nanotubes in the films, we employ a coarse-grained molecular simulation.

In the coarse-grained molecular simulation, each nanotube is modeled as a fiber discretized into a chain of nodes. Neighboring nodes on the same fiber interact to give the bending and stretching stiffness of the nanotube, while nodes on different fibers interact through van der Waals forces (20) (see *Supporting Information*). In this model, the range of AR (1.4-4.2) and f (2-12%) of interest are determined from the characterization results including image processing (25, 27-29). The moduli calculated using the simulation, $E_{1,sim}$ and $E_{2,sim}$, are shown in Fig. 2b. Figure 3 shows that the molecular simulation is

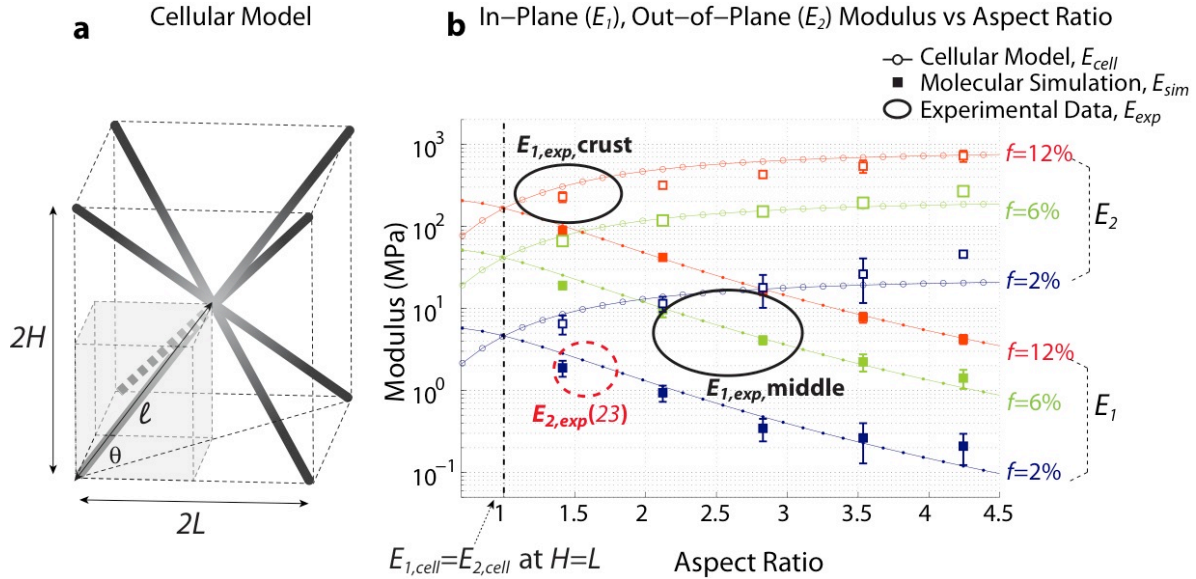


Fig. 2 (a) Schematic of a cellular model unit cell comprised of eight trusses. The gray region depicts the elastic bending of one truss at an angle θ between the vector along the truss and the plane of the horizontal. (b) Predicted in-plane (E_1) and out-of-plane modulus (E_2) using the cellular models (lines) and coarse-grained molecular simulations (squares) with varied AR and f . The error bars of the simulation results represent variations in the modulus over repeated calculations of the same initial conditions. The line colors indicate the different f (2%, 6%, and 12%). The circled regions include the experimental data of single-walled and multi-walled CNT films (25).

qualitatively similar to the SEMs, where the middle layer is more aligned compared to the crust. The average tube orientation θ in the relaxed structure is determined for comparison to the cellular model. Good agreement is observed between the molecular simulations, the cellular model (with a fitting parameter $C=60,000$), and our experimental measurements, as shown in Fig. 2b. The simulation predicts that the moduli in both directions scales with $f^{1.5-2.0}$, depending on the AR, consistent with the f^2 dependence predicted by the cellular model. A film with greater alignment leads to lower $E_{l,sim}$ and higher $E_{2,sim}$ (see *Supplementary Materials*).

The molecular simulations also provide more details about the mechanisms of nanotube deformation when the film is subjected to an elastic strain. There are many complex deformation modes not considered in the cellular model. For example, bundles of nanotubes may move together, a bundle formed by several nanotubes may partially zip (Fig. 4a) or unzip, two nanotubes or bundles may rotate around a contact point (Fig. 4b), and nanotubes within a bundle (oriented perpendicular to the straining direction) may slide relative to each other.

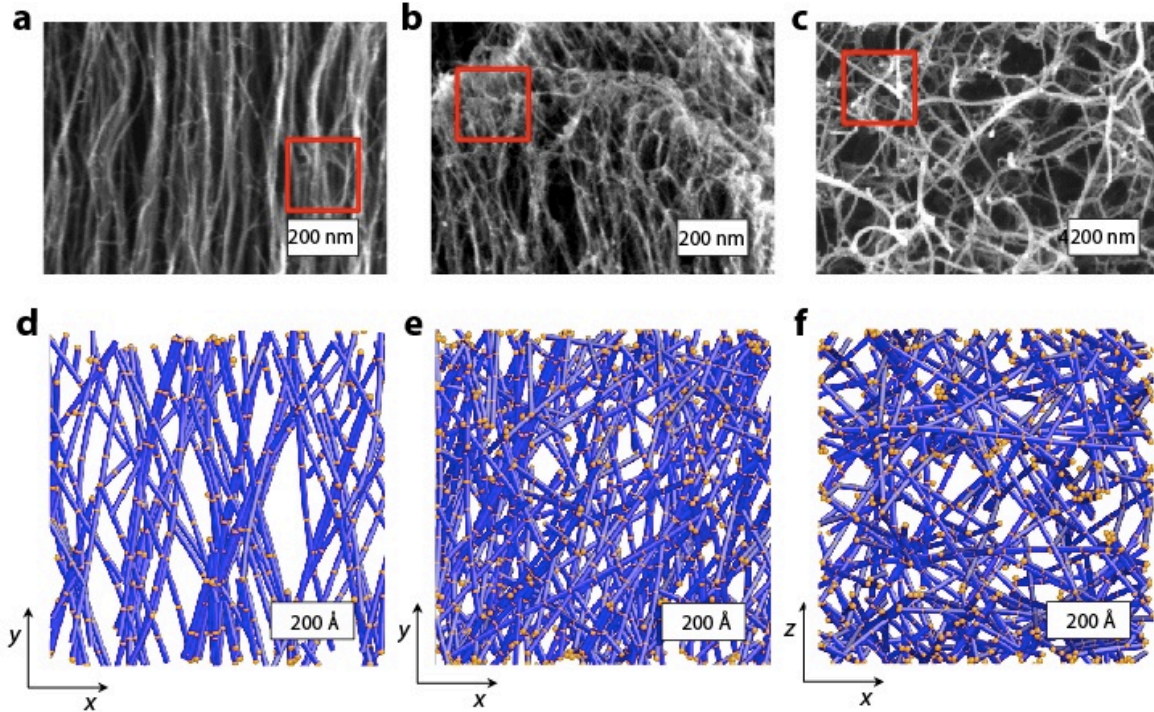


Fig. 3. Examples of SEM images (a-c) and simulation cells ($800\text{\AA} \times 800\text{\AA} \times 400\text{\AA}$) after the relaxation (d-f) of the crust and middle. (a) Cross sectional SEM images of a single-walled CNT film showing aligned nanotubes in the middle region and (b) randomly oriented nanotubes in the crust region, respectively. (c) Top view of the crust layer. The crust has a value of AR of ~ 1.4 and f of 4-8% while the middle layer has AR of 3-5 and f of 2-4%. In the simulations, the nanotubes are constructed using a specific density and orientation to represent the different film morphologies. (d) Simulated aligned nanotubes (AR=4.2, $f=2\%$) and (e) the entangled nanotubes (AR=2.8, $f=4\%$). (f) Top view of the entangled nanotubes (AR=1.4, $f=4\%$).

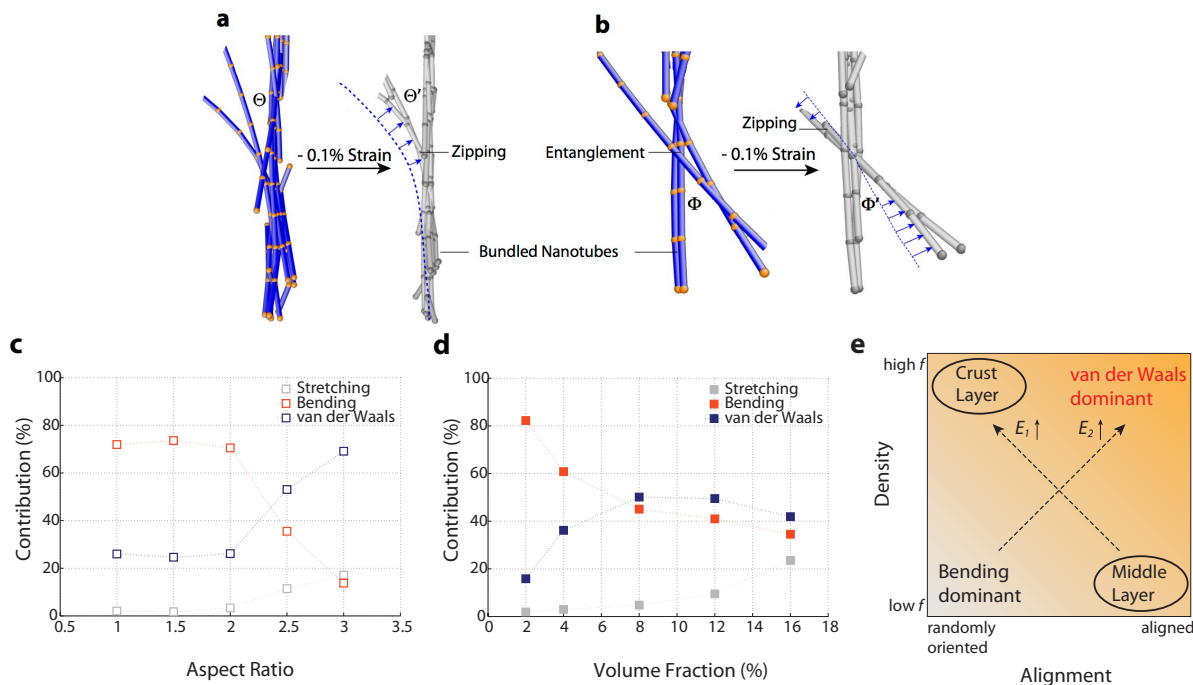


Fig. 4. Nanotube interactions when a compressive 0.1% strain is applied to the film ($f=2\%$, $AR=3.5$). Snapshots from the molecular simulation illustrate the different types of nanotube displacements under strain, including (a) zipping and unzipping (governed by van der Waals forces) and (b) crossed nanotubes. The blue lines show the nanotubes in the initial relaxed structure. The gray lines represent the new positions of the nanotubes when the cell is compressed. The contribution of bending, stretching, and van der Waals energy in the calculation of elastic modulus for varying (c) aspect ratio and (d) volume fraction. (e) Phase diagram to show the governing physics to decide the modulus of nanotubes with varying nanostructures.

To probe the importance of the different deformation mechanisms, we quantify the relative contributions of bending, stretching, and van der Waals energies to the total energy and predicted modulus by measuring the average and curvature of these energy contributions as a function of applied strain, respectively. For most films, the van der Waals energy is the dominant contribution to the total energy of the film, meaning that the energy gained in bundling together nanotubes and forming the film structure during the relaxation steps greatly exceeds the energy cost due to nanotube bending and stretching. However, once the film structure has been formed, either bending energy or van der Waals interaction dominates the effective modulus during applied strain, depending on the CNT morphological details (Fig. 4c and d). For example, for a film of $AR=1.4$ and $f=4\%$, representing the crust layer, the relative contributions of bending, stretching, and van der Waals energies to the total modulus are 72%, 5%, and 23%, respectively. In this case, bending is the dominant contribution in determining the total modulus. However, for a film of $AR=3.5$ and $f=2\%$, representing the middle layer, the contribution of the van der Waals energy to the modulus rises up to 60%. Therefore, the contribution of van der Waals interactions gains importance as the nanotubes become more aligned or as the volume fraction increases, since both effects promote the nanotubes to zip into bundles (Fig. 4e). These results also suggest that the cellular model, which only includes bending forces, is most accurate for structures with low AR and low f (which is the case for many multi-walled CNT samples), though the good agreement between the models suggests that, when fitting parameters are allowed, it is still applicable to higher AR films.

The combination of data and two approaches advances the understanding of the nanostructural effect on the mechanical properties of single-walled CNT films. This understanding is essential for tuning the properties of nanotube films by engineering their nanostructure, which can be achieved by altering the synthesis conditions or by adding surfactant molecules. The development of self consistent simulations and the experimental data can provide guidance on detailed simulation of other material properties including the effective thermal and electrical conductivities. The approach presented here is also applicable to a wide range of films with a fibrous nanostructure, such as films made of nanowires and micro-whiskers.

Methods

Coarse-Grained Nanotube Simulation

We adopt a coarse-grained molecular model in which each nanotube is represented by a set of nodes. The interaction between neighboring nodes on the same chain is designed to reproduce the bending and stretching response of an elastic tube with Young's modulus E_{tube} , inner radius r_{in} , and outer radius r_{out} . A Lennard-Jones (LJ) type interaction is introduced between non-neighboring nodes to account for the van der Waals attraction and steric repulsion between nanotubes. The potential energy as a function of nodal positions $\{r_i\}$ can be written as (26):

$$V(\{r_i\}) = \sum_{(i,j)} \frac{1}{2} k_s (|r_i - r_j| - l_0)^2 + \sum_{(i,j,k)} \frac{1}{2} k_B \left(\frac{(r_i - r_j) \cdot (r_k - r_j)}{|r_i - r_j| |r_k - r_j|} + 1 \right) + \sum_{\langle i,j \rangle} \left(\frac{C_{12}}{|r_i - r_j|^{12}} - \frac{C_6}{|r_i - r_j|^6} \right) \quad (3)$$

The first summation is over all neighboring nodal pairs on the same nanotube; the second summation is over all triplets (i,j,k) in which j is the neighbor of nodes i and k on the same nanotube; the third summation is over all nodal pairs that do *not* belong to the same nanotube. $k_s = E_{tube} A_{tube} / l_0$ and $k_B = E_{tube} I_{tube} / l_0$, where $I_{tube} = \pi(r_{out}^4 - r_{in}^4) / 4$ is the moment of inertia of the tube cross section, and l_0 is the discretization length of the nanotubes. Here we adopt $r_{out} = 5 \text{ \AA}$, $r_{in} = 4.4 \text{ \AA}$ by using the effective tube thickness (30). The LJ coefficients between the nodes are proportional to the LJ coefficients describing the interaction between individual carbon atoms. Specifically, $C_{12} = N_c c_{12}$ and $C_6 = N_c c_6$, where N_c is the number of carbon atoms represented by each node (26), $c_{12} = 2516582.4 \text{ kcal} \cdot \text{mol}^{-1} \text{ \AA}^{12}$, and $c_6 = 1228.8 \text{ kcal} \cdot \text{mol}^{-1} \text{ \AA}^6$ (31, 32). For single-walled CNTs, we estimate N_c to be $2\pi r_{out} l_0 / A_c$, where A_c is the average area covered by each carbon atom. The nanotubes are initialized as straight lines randomly positioned in the simulation cell. The number of nanotubes and the length of each nanotube are selected to achieve the desired density. The initial nanotube orientations are parallel to vector $t = (x_1, x_2 + p, x_3)$, where x_1, x_2 , and x_3 are random numbers uniformly distributed in $[-0.5, 0.5]$. A larger p value corresponds to a stronger alignment to the y -axis. The structure is then allowed to relax by minimizing the potential energy using the conjugate gradient algorithm. During the relaxation, the nanotubes bend and bundle together. The relaxation algorithm stops when the potential energy change in one iteration is smaller than 10^{-4} eV .

After the structure has been relaxed, the components of the elastic stiffness tensor (C_{ij}) connecting normal stress (σ_i), and normal strain (ϵ_j) (where $\sigma_i = C_{ij} \epsilon_j$) are computed by stretching the simulation cell along the x , y , and z axes, respectively, relaxing the structure again and computing the stress change. The maximum strain applied to the simulation cell is $\pm 0.1\%$, which is also the maximum applied strain in our experiments. The effective modulus of $E_{1,sim}$ and $E_{2,sim}$ are computed from the components of the elastic stiffness tensor. For example, $E_{1,sim}$ corresponding to the equivalent value of $E_{1,exp}$ in the current work is

$$E_{1,sim} = C_{11} - (C_{11}C_{12} - C_{12}C_{13})(C_{11}C_{12} - C_{12}^2)^{-1} C_{12} - (C_{12}^2 - C_{13}C_{22})(C_{12} - C_{11}C_{22})^{-1} C_{13} \quad (4)$$

where σ_y and σ_z are assumed to be zero because of the free surfaces of the single-walled CNT films. Since VACNT films have entangled morphologies showing foam-like behavior (12, 33), we assume that the film has a Poisson's ratio of zero. Thus the $E_{2,sim}$ is assumed to be C_{22} .

The model accounts for the nanotube morphology by incorporating various density and alignment parameters (*i.e.* AR and f). The coarse-grained molecular simulation predicts the mechanical response of single-walled CNT films depending on the film nanostructures and the intrinsic mechanical behavior of nanotubes.

Acknowledgements: This work was sponsored by the Office of Naval Research (N00014-09-1-0296-P00004) the National Science Foundation, and the Semiconductor Research Corporation. W.C. acknowledges support from the NSF Grant CMS-0547681. S.M. acknowledges financial support from Grant-in-Aid for Scientific Research (19054003 and 22226006), and Global COE Program. We performed this work in part at the Stanford Nanofabrication Facility, which is supported by the NSF under Grant ECS-Integrated Systems.

Author contributions: K.G. proposed and supervised the project, Y.W. and T.K. designed the experiments, Y.W. carried out the experiments, Y.W., Y.G. and W.C. worked on the physical models, Y.W. and W.C. developed the simulations, R.X. and S.M. grew the CNT films, and Y.W., Y.G., W.C., and K.G. wrote the manuscript. All the authors participated in discussions of the research. The authors declare no conflict of interest.

References

1. Ge L, Sethi S, Ci L, Ajayan PM, Dhinojwala A (2007) Carbon nanotube-based synthetic gecko tapes. *Proceedings of the National Academy of Sciences of the United States of America* 104:10792–10795.
2. Bell LE (2008) Cooling, Heating, Generating Power, and Recovering Waste Heat with Thermoelectric Systems. *Science* 321:1457–1461.
3. Baughman R, Zakhidov A, De Heer W (2002) Carbon nanotubes--the route toward applications. *Science* 297:787.
4. Balandin AA (2011) Thermal properties of graphene and nanostructured carbon materials. *Nature materials* 10:569–581.
5. Goodson K (2007) Ordering Up the Minimum Thermal Conductivity of Solids. *Science* 1138067:315.
6. Gao Y et al. (2010) Nanostructured Interfaces for Thermoelectrics. *Journal of Electronic Materials* 39:1456–1462.
7. Prasher R (2006) Thermal interface materials: historical perspective, status, and future directions. *Proceedings of the IEEE* 94:1571–1586.
8. Marconnet AM, Panzer MA, Goodson KE (2013) Thermal Conduction Phenomena in Carbon Nanotubes and Related Nanostructured Materials. *Reviews of Modern Physics*:1–49.
9. Tong T et al. Dense Vertically Aligned Multiwalled Carbon Nanotube Arrays as Thermal Interface Materials. *IEEE Trans Comp Packag Technol* 30:92–100.
10. Cao A, Dickrell PL, Sawyer WG, Ghasemi-Nejhad MN, Ajayan PM (2005) Super-compressible foamlike carbon nanotube films. *Science* 310:1307–1310.
11. Panzer M et al. (2008) Thermal Properties of Metal-Coated Vertically Aligned Single-Wall Nanotube Arrays. *Journal of Heat Transfer* 130:052401.
12. Maschmann MR, Zhang Q, Du F, Dai L, Baur J (2011) Length dependent foam-like mechanical response of axially indented vertically oriented carbon nanotube arrays. *Carbon* 49:386–397.
13. Olofsson N, Ek-Weis J, Eriksson A, Idda T, Campbell E (2009) Determination of the effective Young's modulus of vertically aligned carbon nanotube arrays: a simple nanotube-based varactor.

Nanotechnology 20:385710.

14. Deck C, Flowers J, McKee G, Vecchio K (2007) Mechanical behavior of ultralong multiwalled carbon nanotube mats. *Journal of Applied Physics* 101:023512.
15. Won Y et al. (2012) Mechanical characterization of aligned multi-walled carbon nanotube films using microfabricated resonators. *Carbon* 50:347–355.
16. Bedewy M, Meshot ER, Reinker MJ, Hart AJ (2011) Population Growth Dynamics of Carbon Nanotubes. *ACS nano* 5:8974–8989.
17. Zhang L et al. (2006) Influence of a top crust of entangled nanotubes on the structure of vertically aligned forests of single-walled carbon nanotubes. *Chemistry of materials* 18:5624–5629.
18. Terrones M, H Terrones, Banhart F, J-C Charlier, Ajayan PM (2000) Coalescence of Single-Walled Carbon Nanotubes. *Science* 288:1226–1229.
19. Xu M, Futaba DN, Yamada T, Yumura M, Hata K (2010) Carbon Nanotubes with Temperature-Invariant Viscoelasticity from -196 to 1000 C. *Science* 330:1364–1368.
20. Buehler MJ (2006) Mesoscale modeling of mechanics of carbon nanotubes: Self-assembly, self-folding, and fracture. *Journal of Materials Research* 21:2855–2869.
21. Won Y et al. (2012) Crust removal and effective modulus of aligned multi-walled carbon nanotube films. *Proceedings of the Thirteenth InterSociety Conference on Thermal and Thermomechanical Phenomena in Electronic Systems* :1070–1076.
22. Murakami Y et al. (2004) Growth of vertically aligned single-walled carbon nanotube films on quartz substrates and their optical anisotropy. *Chemical Physics Letters* 385:298–303.
23. Bedewy M et al. (2009) Collective mechanism for the evolution and self-termination of vertically aligned carbon nanotube growth. *The Journal of Physical Chemistry C* 113:20576–20582.
24. Gibson L, Ashby M (1999) *Cellular solids: structure and properties* (Cambridge Univ Pr).
25. Gao Y et al. (2012) Impact of nanotube density and alignment on the elastic modulus near the top and base surfaces of aligned multi-walled carbon nanotube films. *Carbon* 50:3789–3798.
26. Harik V (2002) Mechanics of carbon nanotubes: applicability of the continuum-beam models. *Computational materials science* 24:328–342.
27. Xiang R et al. (2008) Growth deceleration of vertically aligned carbon nanotube arrays: Catalyst deactivation or feedstock diffusion controlled? *The Journal of Physical Chemistry C* 112:4892–4896.
28. Weisman RB, Bachilo SM (2003) Dependence of Optical Transition Energies on Structure for Single-Walled Carbon Nanotubes in Aqueous Suspension: An Empirical Kataura Plot. *Nano Letters* 3:1235–1238.
29. Yakobson B (2004) Carbon nanotubes: Supramolecular mechanics. *Dekker Encyclopedia of Nanoscience and Nanotechnology*:587–601.
30. Yakobson B, Brabec C, Bernholc J (1996) Nanomechanics of carbon tubes: instabilities beyond linear response. *Physical Review Letters* 76:2511–2514.

31. Jones J (1924) On the Determination of Molecular Fields. III. From Crystal Measurements and Kinetic Theory Data. *Proceedings of the Royal Society of London Series A* 106:709–718.
32. Waals J, Kohnstam P (1908) *Lehrbuch der Thermodynamik, Mass and Van Suchtelen, Leipzig, Part I* (books.google.com).

Figure Legends

Fig. 1. (a) Effective in-plane modulus ($E_{1,exp}$) of vertically aligned single-walled CNT samples measured using a resonator technique. The thickness variations and the resulting modulus variations due to the nonuniformities in nanotube growth are illustrated by the horizontal and vertical error bars, respectively. (Inset) Schematic of a resonator with a vertically aligned CNT film and a schematic showing the different layers in a film are overlaid on the plot.

(b) Dimensionless modulus $E^* = \frac{E_{CNT}}{E_{ref}} \frac{\rho_{ref}}{\rho_{CNT}}$, including our past data on multi-walled CNT films (15, 21) and

best-fit lines calculated using a three-layer analysis. Dashed lines indicate the effect of varying modulus of the crust (600 MPa) and middle (10 MPa) layers by $\pm 10\%$ on the effective modulus.

Fig. 2 (a) Schematic of a cellular model unit cell comprised of eight trusses. The gray region depicts the elastic bending of one truss at an angle θ between the vector along the truss and the plane of the horizontal. (b) Predicted in-plane (E_1) and out-of-plane modulus (E_2) using the cellular models (lines) and coarse-grained molecular simulations (squares) with varied AR and f . The error bars of the simulation results represent variations in the modulus over repeated calculations of the same initial conditions. The line colors indicate the different f (2%, 6%, and 12%). The circled regions include the experimental data of single-walled and multi-walled CNT films (25)

Fig. 3. Examples of SEM images (a-c) and simulation cells ($800\text{\AA} \times 800\text{\AA} \times 400\text{\AA}$) after the relaxation (d-f) of the crust and middle. (a) Cross sectional SEM images of a single-walled CNT film showing aligned nanotubes in the middle region and (b) randomly oriented nanotubes in the crust region, respectively. (c) Top view of the crust layer. The crust has a value of AR of ~ 1.4 and f of 4-8% while the middle layer has AR of 3-5 and f of 2-4%. In the simulations, the nanotubes are constructed using a specific density and orientation to represent the different film morphologies. (d) Simulated aligned nanotubes (AR=4.2, $f=2\%$) and (e) the entangled nanotubes (AR=2.8, $f=4\%$). (f) Top view of the entangled nanotubes (AR=1.4, $f=4\%$).

Fig. 4. Nanotube interactions when a compressive 0.1% strain is applied to the film ($f=2\%$, AR=3.5). Snapshots from the molecular simulation illustrate the different types of nanotube displacements under strain, including (a) zipping and unzipping (governed by van der Waals forces) and (b) crossed nanotubes. The blue lines show the nanotubes in the initial relaxed structure. The gray lines represent the new positions of the nanotubes when the cell is compressed. The contribution of bending, stretching, and van der Waals energy in the calculation of elastic modulus for varying (c) aspect ratio and (d) volume fraction. (e) Phase diagram to show the governing physics to decide the modulus of nanotubes with varying nanostructures.